CrossMark

ARTICLE

Evolution of microstructure and mechanical properties in Zn–Cu–Ti alloy during severe hot rolling at 300 °C

Shengya Ji
Faculty of Materials Science and Engineering, Xi'an University of Technology, Xi'an 710048, China; School of Materials Science and Engineering, Henan University of Science and Technology, Luoyang 471023, China; and Department of Materials Engineering, Henan Institute of Technology, Xinxiang 453003, China

Shuhua Liang
Faculty of Materials Science and Engineering, Xi'an University of Technology, Xi'an 710048, China

Kexing Song[a] and Hongxia Li
School of Materials Science and Engineering, Henan University of Science and Technology, Luoyang 471023, China

Zhou Li
School of Materials Science and Engineering, Central South University, Changsha 410083, China

(Received 7 March 2017; accepted 26 June 2017)

The present investigation aims to explore the evolution of microstructure and mechanical properties in Zn–Cu–Ti alloys during severe hot-rolling deformation. Twin deformation and dynamic recrystallisation are two important deformation modes of Zn–Cu–Ti alloys during hot rolling at 300 °C. Twin deformation and dynamic recrystallisation (DRX) appear one after the other. They not only consume the deformation stored energy but also inhibit initiation and growth of cracks. The elongation rate of Zn–Cu–Ti alloys has a rising trend with the increase in hot-rolling deformation. It is mainly due to grain refinement caused by increasing the ratio of DRX and twin deformation. The tensile strength of Zn–Cu–Ti alloys is found to decrease with the increase in hot-rolling deformation. This is because the solid-solution strengthening effect of copper is weakened by more deformation-induced precipitation of ε phase ($CuZn_5$). The solid-solution strengthening effect of copper plays an important role in the strengthening effect of Zn–Cu–Ti alloys.

I. INTRODUCTION

As a kind of thermal mechanical deformation process, hot rolling has the advantage of high-production efficiency. It is suitable not only for continuous and automated industrial processes but also for large-scale industrial production. It has become an indispensable step in processing zinc–copper–titanium (Zn–Cu–Ti) alloy sheets. At present, it has also become highlighted in the world that ultrafine-grained alloys are prepared by severe plastic deformation.[1,2] Under the condition of severe plastic deformation, evolution of microstructure and mechanical properties of alloys has a unique rule. Ultrafine equiaxed grains are not only efficiently obtained in the process but the morphology, distribution, and size of the second phase in alloys are changed. In recent years, more attention from scholars has been paid to the research on dissolution and precipitation of the second phase in alloys under the condition of severe plastic deformation.[3,4] What is more, it is generally believed that dislocations in alloys with higher stacking-fault energies (such as Zn, Al, and Mg) are easier to cross slip and climb. Dynamic recovery can eliminate dislocations and subgrain boundaries in the deformed alloys. Accordingly, these materials lack the condition of dynamic recrystallisation (DRX). However, in recent years, DRX has been found in the thermal deformation process of aluminum alloy,[5,6] magnesium alloy,[7] and ferrite alloy.[8] Experiments have shown that DRX really occurred in Zn–Cu–Ti alloys during hot rolling at 300 °C.

Currently, there are few reports about the severe hot-rolling deformation mechanism in Zn–Cu–Ti alloys. Therefore, in this article, we systematically study the evolution of microstructures and mechanical properties in Zn–Cu–Ti alloys with different hot-rolling deformations. Our aim is to contribute not only to the production of Zn–Cu–Ti alloy sheets with uniformity and high plasticity, strength, and ductility but also to the further improvement of the plastic deformation theory of Zn–Cu–Ti alloys.

II. EXPERIMENTAL PROCEDURES

In our experiments, we used Zn with a nominal purity of 99.995 mass% and titanium sponge with a nominal

Contributing Editor: Jürgen Eckert
[a]Address all correspondence to this author.
e-mail: kxsong@haust.edu.cn
DOI: 10.1557/jmr.2017.275

 © Materials Research Society 2017

https://doi.org/10.1557/jmr.2017.275 Published online by Cambridge University Press

purity of 99.7 mass%. Cu was obtained from brass, the composition of which was 68% Cu and 32% Zn. The composition of the investigated alloy is Zn–1.5Cu–0.05Ti–0.002Mg. These materials were melted in a graphite crucible in a ZGJL0.01-4C-4 vacuum induction furnace (Jinzhou Electric Furnace Company, Jinzhou, China). The alloy was melted by electromagnetic induction under an argon flow to prevent oxidation.

After being poured, the alloy was extruded into a slab, which was then cut into a right-angle trapezoid by a wire-cutting equipment. One end of the right-angle trapezoid slab was 7 mm thick, and the thickness transitioned uniformly to the other end, which was 1 mm thick. Before rolling the slab, we made marks at the different slab thickness positions. After rolling, alloy sheets with different deformations were cut into 1 × 1 × 2 mm samples by wire-cutting equipments. The samples were ground into 30-μm thin slices by different types of sandpaper. The slices were stamped into 3-mm diameter wafers. Finally, the wafers were thinned by a Gatan particle-thinning apparatus. A transmission electron microscope (TEM; model JEM-2100, JEOL Ltd., Tokyo, Japan) was used to detect the microstructural features of the Zn–Cu–Ti alloys.

According to the technical requirements of GB3076-1982 (Standard Test Method for Tensile Testing of Metallic Sheet or Strip) and GB5027 (Standard Test Method for Plastic Strain Ratio "*r* value" of Metal Sheet), the tensile sample was cut to be 2 mm thick by a wire-cutting equipment. Besides, shape and dimensions were required to be identical with Fig. 1 (mm). Before the tensile test, to improve the veracity of the tensile data, oil pollution caused by wire cutting was cleaned on the surface of the samples. Moreover, transverse sections of the samples were polished by different types of sandpapers till there was no groove. A precision universal testing machine (Model SHIMADZU AG-I250KN, Shimadzu (China) Co., Ltd., Beijing, China) was used to detect the mechanical properties of the alloy.

Beer–Lambert law[9]:

$$A = \lg\left(\frac{1}{T}\right) = K \cdot b \cdot c \qquad (1)$$

Equation: A stands for the light absorption degree, T for the transmission rate (the rate of the projection light intensity and the incident light intensity), K for the molar absorption coefficient, c for the concentration of light-absorbing material, and b for the thickness of absorption layer. From Formula (1), it can be seen that there is an exponential relationship between A (for the light absorption degree) and T (for the transmission rate), and there is also a linear relationship between A (for the light absorption degree) and c (for the concentration of light-absorbing material). A exactly refers to Density Optical. The brightness of the second phase in the alloy determines its optical density in the metallograph of the alloy. Meanwhile, its optical density further determines its own gray level (light and shade degree of the second phase particles in the alloy) in the metallograph. In theory, there is a positive correlation between the optical density of the metallograph and the brightness of the second phase. Therefore, according to the brightness and size of the metallograph, the Image-Pro Plus analysis software (Media Cybernetics, Bethesda, Maryland) is used to make a quantitative measurement of the second phase in the alloy.

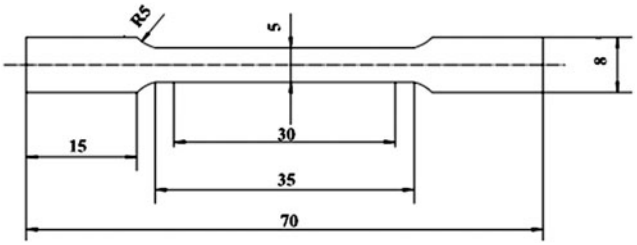


FIG. 1. Schematic diagram of tensile samples.

III. RESULTS AND DISCUSSION

A. Microstructural observations: DRX mechanical evolution

DRX includes two processes, nucleation and growth, which are similar to static recrystallisation during annealing after cold deformation.[10] Deformation-stored energy is the driving force of DRX nucleation.[11] DRX of an alloy is influenced mainly by two factors: internal factors (mechanical properties of the alloy, grain size, and the pinning effect of the second-phase particles on grain boundaries) and external factors (deformation temperature and deformation velocity).

During hot rolling of Zn–Cu–Ti alloys, twin deformation and DRX appear one after the other. They not only consume the deformation-stored energy but also inhibit initiation and growth of cracks. In this study, we examined the nucleation and growth regularity of twins and DRX during hot rolling of Zn–Cu–Ti alloys.

As shown in Fig. 2(a), primary twins appeared in the alloy. The grains were separated by primary twins, which played the role of grain refinement. It was found that high-density dislocations appeared in the alloy, as shown in Fig. 2(b). The dislocation grid was formed by these mutually entangling dislocations. Thus, it can be seen that the driving force of DRX is insufficient due to the smaller deformation. The deformation mechanism of Zn–Cu–Ti alloys at the 33.3% deformation is mainly a local dislocation motion and an entanglement, complementary with the twin deformation.

Primary twins appeared in the alloy [see Fig. 2(c)]. As shown in Fig. 2(d), dislocations began to move under the influence of internal stress. During this movement, some parts of the dislocations in the opposite direction to the

https://doi.org/10.1557/jmr.2017.275 Published online by Cambridge University Press

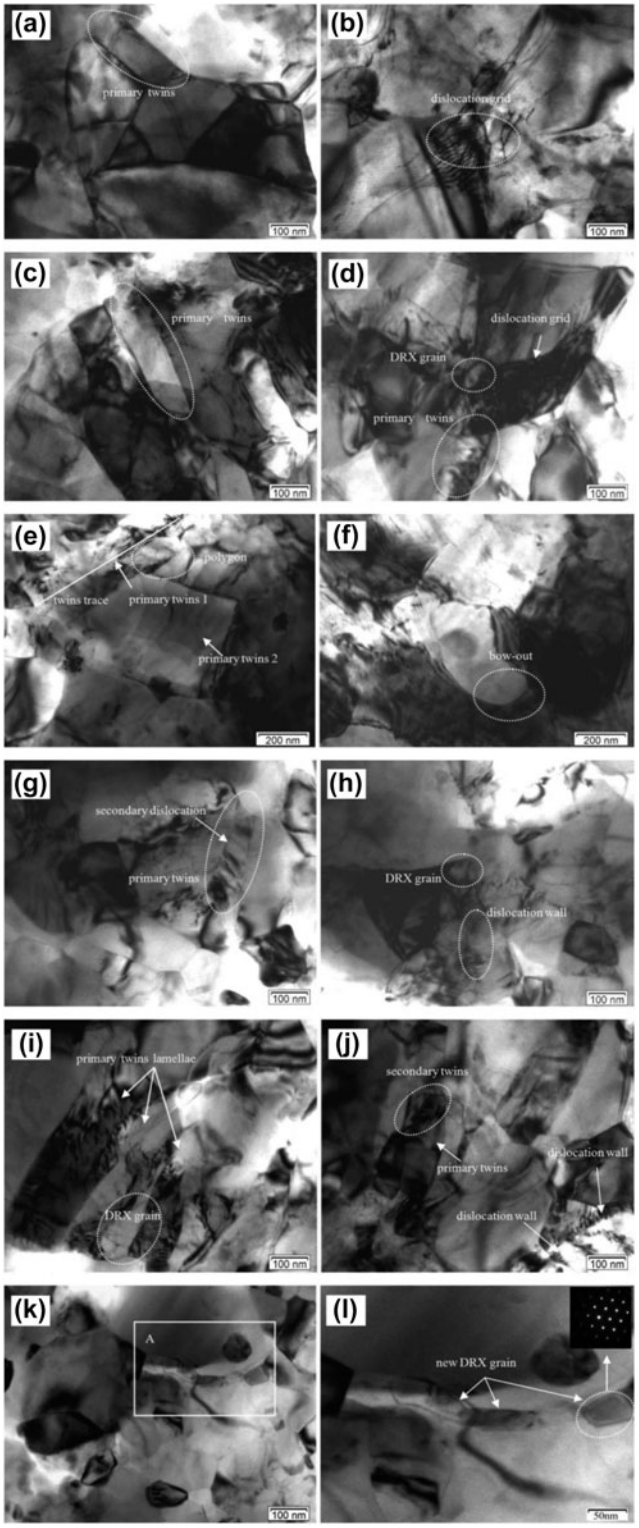


FIG. 2. TEM characterisation of as-rolled Zn–Cu–Ti alloy sheet with different hot-rolling deformations at 300 °C: (a, b) 33.3%, (c, d) 50%, (e, f) 60%, (g, h) 66.6%, and (i, j, k, l) 71.4%.

Burgers vector collided and were annihilated, and other parts of the dislocations in the same direction as the Burgers vector collided, entangled with each other, and reorganized into some orderly dislocation grid, the process of which is known as dynamic recovery. Under the segmentation action of the dislocation grid, the DRX grain clearly appears in the grain interior [see Fig. 2(d)]. The interior of the DRX grain is relatively bright compared with its interface. This is because the dislocations were absorbed and reorganized by the DRX grain. With the increase in the deformation, the dislocation source will transmit more dislocations. The proliferative dislocations will accumulate and reorganize at the interface of the DRX grain. The DRX grain will gradually grow, which is called the continuous dynamic recrystallization (CDRX). Data shows that CDRX has three stages[12]: dislocation proliferation, dynamic recovery, and an increase in orientation difference in small-angle grain boundaries. Due to the limitation of experimental conditions, the growth of small-angle interface cannot be observed.

Two primary twins crossed each other [see Fig. 2(e)], and dislocation walls appeared in the interior of primary twins 1. A polygon was generated by the entanglement, and gathering of dislocations occurred in the interior of primary twins 1, which is called the twins' dynamic recrystallisation (TDRX). Polygon boundaries were formed by the dislocation wall and primary twins 1 boundary. As shown in Fig. 2(e), TDRX nucleation in the Zn–Cu–Ti alloy was formed by dislocation reorganisation of the primary twins 1 interior.

Reports[13–15] show that TDRX has three possible ways to nucleate: nucleation in the mutual intersection area of primary twins [see Fig. 3(a)], the direct nucleation of secondary twins [see Fig. 3(b)], and the direct nucleation of small-angle grain boundaries in the twins' interiors [see Fig. 3(c)].

Under the conditions of high temperature and a medium hot-rolling deformation, critical shear stress of dislocation slip was reduced, the diffusion ability of the atoms was enhanced, and the sliding and moving rates of the grain boundary were correspondingly increased. The original grain boundary moved because the of dislocation slip, which caused the grain boundary bow out [see Fig. 2(f)]. A very irregular grain boundary was produced in the original grain boundary, which is called the discontinuous dynamic recrystallization (DDRX).

Statistics show that the grain boundary bow out is the nucleation site of the DDRX.[16,17] To coordinate the larger stress-gradient difference near the bow-out interface, the dislocation source in the grain boundary sends nonbasal dislocations to the grain interior. With the mutual intersections of basal and nonbasal dislocations, the bow out in the grain boundary is divided to form a subgrain boundary. The neighboring dislocations keep moving, entangling, and gathering in the subgrain boundary until they are absorbed by it. Finally, the small-angle subgrain boundary grows into a large-angle grain

https://doi.org/10.1557/jmr.2017.275 Published online by Cambridge University Press

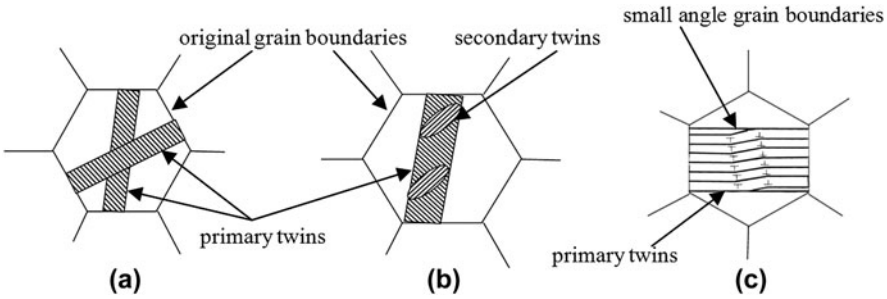


FIG. 3. Schematic diagram of the TDRX mechanism.[13–15] (a) Nucleation in the mutual intersection area of primary twins, (b) direct nucleation of secondary twins, and (c) direct nucleation of small-angle grain boundaries.

boundary. It is known from the analyses above that, under the conditions of high temperatures and a medium hot-rolling deformation, the DRX mechanism of Zn–Cu–Ti alloys has a tendency to diversify.

With the increase in the hot-rolling deformation (66.6%), high-density secondary dislocations appeared in the primary twins [see Fig. 2(g)]. Under the cutting action of the secondary dislocations, the interiors the of primary twins were divided into small grains. The border of a small grain comprised of both dislocations and primary-twin boundaries. Under the segmentation action of dislocations, the dislocation wall and the DRX grain clearly appeared in the interiors of grains [see Fig. 2(h)].

With the continuous increase in the hot-rolling deformation (71.4%), TEM morphology shows that primary twins' lamellae were formed by four parallel primary twins [see Fig. 2(i)]. High-density dislocations appeared in every primary twin's lamella. Through the further absorption and reorganisation of dislocations, The DRX grain was formed in the interiors of the primary twins' lamellae [see Fig. 2(i)]. In Fig. 2(j), these dislocation walls were formed by entangled high-density dislocations. The matrix (η phase) was cut into some relatively independent DRX grains by those dislocation walls.

Secondary twins clearly appeared in the primary twins [see Fig. 2(j)]. Only when the number of primary twins reached a certain proportion, can the secondary dislocations and secondary twins occur in primary twins during the plastic deformation process of an alloy.[18–20] The conclusion can be drawn from Fig. 2(j) that the primary twin density of the alloy reached a higher value after the deformation of Zn–Cu–Ti alloys was up to 71.4%.

Figure 2(l) is the amplification of the local rectangular area *A* in Fig. 2(k). Secondary DRX began to nucleate and grow along the original DRX grain boundaries [see Figs. 2(k) and 2(l)]. Dislocations cannot be seen in the original DRX grains [see Fig. 2(l)]. The original DRX grains interior is relatively bright. Secondary DRX grains appeared at the intersection of the adjacent grain boundaries, which inhibited the further growth of the original DRX grains. Belyakov and Miura[21,22] believe that secondary DRX is closely related to the grain boundary slip. When the grain boundary slip is blocked at the triple grain boundary, stress concentration is produced there. When the deformation-stored energy at the triple grain boundary increases to a certain extent, new nucleation and growth will occur again.

From the above analysis, it can be found that under the condition of small deformations (33.3–60%), CDRX and DDRX are the main deformation mechanisms, complemented with twin deformation at the early stage of deformation. Under the condition of medium and high deformations (66.6–71.4%), twin deformation and TDRX are the main deformation mechanisms, complemented with CDRX. The matrix (η phase) in Zn–Cu–Ti alloys is further refined with the increase in hot-rolling deformation. This is because the twin nucleation is faster than proliferation, movement, and reorganization of dislocations. In addition, higher deformation-stored energy is produced by the severe plastic deformation, which induces secondary DRX. It also contributes to the further refinement of grains in Zn–Cu–Ti alloys.

B. Morphology evolution of ε phase ($CuZn_5$)

The Zn–Cu–Ti alloy is mainly composed of η phase, $TiZn_{16}$ phase, and ε phase ($CuZn_5$). $TiZn_{16}$ phase is not easy to be distinguished in the metallographic structure of the alloy. It can be attributed to its little content. The standard electrode potential of Zn is −0.763 E/V and Cu is 0.337 E/V. Relative to the matrix (η phase), a corrosion galvanic cell was easily formed in the ε phase ($CuZn_5$). And ε phase ($CuZn_5$) was corroded black by metallographic corrosive liquids. As shown in Fig. 4(a), the microstructure of Zn–Cu–Ti alloy sheets with 33.3% deformation is mainly composed of white matrix (η phase) and black ε phase ($CuZn_5$). Under the compressive stress of hot rolling, local stress accumulation was produced in the grain interior of ε phase ($CuZn_5$). Dislocations within the grains of ε phase entangled with each other, and dislocation slip was hindered and inhibited. Finally, dislocations across the interior of ε phase ($CuZn_5$) were triggered by the local stress accumulation, which led to the breakage and fracture of ε phase

https://doi.org/10.1557/jmr.2017.275 Published online by Cambridge University Press

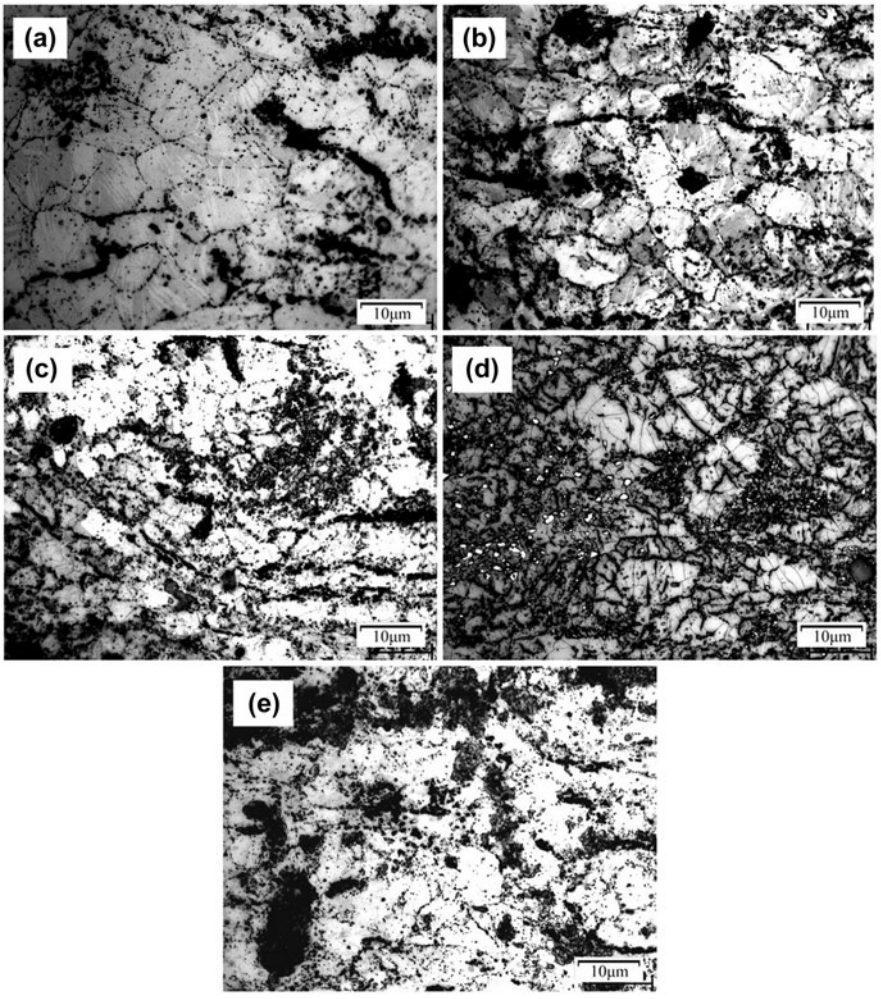


FIG. 4. OM micrographs of as-rolled Zn–Cu–Ti alloy sheet with different hot-rolling deformations at 300 °C: (a) 33.3%, (b) 50%, (c) 60%, (d) 66.6%, and (e) 71.4%.

($CuZn_5$). Some parts of ε phase ($CuZn_5$) were broken into granules and unevenly distributed in the matrix along the grain boundaries. Other parts of ε phase ($CuZn_5$) were distributed in the matrix in the shape of a block-like, chain-like, and band-like aggregation along the rolling direction.

In Zn–Cu–Ti alloy sheets with 50% deformation, ε phase ($CuZn_5$) is distributed in the matrix (η phase) along the rolling direction in the shape of a black globle-like and band-like aggregation [see Fig. 4(b)]. In comparison to Zn–Cu–Ti alloy with 33.3% deformation [see Fig. 4(a)], the morphology of ε phase ($CuZn_5$) gradually evolved from black band-like aggregation to stubby block-like and globe-like aggregations. Most of the broken ε phase ($CuZn_5$) is distributed along the grain boundary, while a small amount of broken ε phase ($CuZn_5$) scattered in the matrix (η phase). The enrichment zone [see large black area shown in Fig. 4(b)] and nonenrichment zone [see large white area shown in Fig. 4(b)] of ε phase ($CuZn_5$) can be clearly distinguished in the metallograph.

As shown in Fig. 4(c), in Zn–Cu–Ti alloy sheets with 60% deformation, ε phase ($CuZn_5$) in the shape of band-like aggregations is diffused and expanded along the vertical rolling direction. The trend of evolution from band-like aggregations to stubby block-like and globe-like aggregations became more obvious. A large amount of ε phase ($CuZn_5$) in the shape of point-like and globe-like aggregations increased. In comparison to Zn–Cu–Ti alloys with 50% deformation, the degree of dispersion of ε phase ($CuZn_5$) was further improved.

As can be seen from Fig. 4(d), in Zn–Cu–Ti alloy sheets with 66.6% deformation, ε phase ($CuZn_5$) in the matrix (η phase) is distributed more diffusely. Under the compressive stress of hot rolling, ε phase ($CuZn_5$) was gradually broken and reunited to be stubby block-like aggregations and granular in the matrix (η phase) [see Fig. 4(d)]. Although the enrichment zone and nonenrichment zone of ε phase ($CuZn_5$) can be clearly distinguished in the metallograph. The contrast ratio of different regions of the metallograph (black and white

https://doi.org/10.1557/jmr.2017.275 Published online by Cambridge University Press

contrast or color difference of adjacent parts) decreased significantly.

As shown in Fig. 4(e), in Zn–Cu–Ti alloy sheets with 71.4% deformation, ε phase ($CuZn_5$) is unevenly distributed in the matrix (η phase). Under the compressive stress of hot rolling, some parts of ε phase ($CuZn_5$) were broken and reunited to be line-like, rod-like and band-like distributions in the matrix (η phase). And other parts of ε phase ($CuZn_5$) were gradually broken and reunited to be stubby block-like and globe-like aggregations in the matrix (η phase). In comparison to Zn–Cu–Ti alloy with 66.6% deformation, the contrast ratio of different regions of metallograph (black and white contrast or color difference of adjacent part) increased significantly. The degree of dispersion of ε phase ($CuZn_5$) in the matrix (η phase) was further decreased. It can be attributed to the short rolling time and severe rolling deformation.

It can be seen from Fig. 2 that twin deformation occurred in the matrix. The deformation twins, however, cannot be clearly distinguished in the metallograph [see Fig. 4]. This is because, on the one hand, deformation twins in Zn–Cu–Ti alloys are small in size. And what's more, the color of deformation twins in the metallograph is close to that of ε phase ($CuZn_5$). On the other hand, the difficulty level of slip system initiation is mainly dependent on critical shear stress, and the slippage is mainly dependent on dislocation character of the slip plane.[25] The higher the plastic deformation temperature, the greater the activation energy of atoms and the smaller the binding force between atoms. Heat was produced by deformation and friction during the hot-rolling process, which led to the rising temperature of Zn–Cu–Ti alloy sheets. As for Zn–Cu–Ti alloys endowed with close-packed hexagonal crystal lattices, critical shear stress of nonbasal slip decreases with the rising temperature. When the plastic deformation temperature rises up higher than 300 °C, critical shear stress of the prismatic slip $\{10\bar{1}0\}\langle 11\bar{2}0\rangle$ and pyramidal slip $\{11\bar{2}2\}\langle 11\bar{2}3\rangle$ sharply falls. Critical shear stress of them is close to that of the basal slip.[23] Thus, when the plastic deformation temperature rises up, both prismatic slip and pyramidal slip of Zn–Cu–Ti alloys endowed with close-packed hexagonal crystal lattices are activated. Moreover, nucleation of deformation twins belongs to the stress activation. Shear resistance of the grain boundary decreases with the rising temperature. The local stress concentration caused by uneven deformation is released by prismatic slip, pyramidal slip, and grain boundary sliding, which is not advantageous to nucleation of the deformation twins,[24–26] and the probability of DRX is greatly increased.

From the above analysis, it can be found that the changes in morphology and distribution of ε phase ($CuZn_5$) can be divided into three stages. In the small rolling deformation (from 33.3 to 50%), its morphology gradually evolves from the large lump and uneven band-like aggregation distribution to the globe-like, granular, and line-like aggregation distribution. In the moderate rolling deformation (from 60 to 66.6%), the aggregation distribution of ε phase ($CuZn_5$) is not only elongated along the rolling direction, but it is also diffused and swollen along the vertical rolling direction. When the deformation reached 66.6%, ε phase ($CuZn_5$) was completely dispersed in the matrix, and its morphology became more tiny globe-like and granular. The continuous or discontinuous network of ε phase ($CuZn_5$) distributes on the grain boundary of the matrix (η phase). In the large rolling deformation (71.4%), the degree of dispersion of ε phase ($CuZn_5$) in the matrix (η phase) further decreases, and some parts of ε phase ($CuZn_5$) are broken and reunited to be line-like distributions in the matrix (η phase).

In comparison with Fig. 4, it can be seen that amounts of ε phase ($CuZn_5$) had a rising trend with the increase in hot-rolling deformation. It is mainly due to deformation-induced precipitation of ε phase ($CuZn_5$) produced in the process of hot-rolled Zn–Cu–Ti alloys. Mechanical properties of Zn–Cu–Ti alloys are influenced by the amount, morphology, and distribution of ε phase ($CuZn_5$). Therefore, it is indispensable and valuable to make a quantitative research on the effect of hot-rolling deformation on deformation-induced precipitation of ε phase ($CuZn_5$).

C. Deformation-induced precipitation of ε phase ($CuZn_5$)

By comparison of ellipse regions in Figs. 5(a)–5(c), it can be found that new diffraction peaks of ε phase ($CuZn_5$), respectively, appear in as-extruded and as-rolled Zn–Cu–Ti alloys. Moreover, the new diffraction peak of ε phase ($CuZn_5$) in as-rolled Zn–Cu–Ti alloys was significantly higher than that in as-extruded Zn–Cu–Ti alloys. This suggests that the deformation-induced precipitation of ε phase ($CuZn_5$) occurred in both hot-extruding and hot-rolling processes. In Fig. 5(d), it cannot be seen clearly that intensity of new diffraction peaks of ε phase ($CuZn_5$) has a rising trend with the increase in rolling deformation.

In Fig. 5(d), the intensity of new diffraction peaks of ε phase was measured using the ImageJ software. Table I is the corresponding value of Fig. 5(d). Intensity of new diffraction peaks of ε phase has a rising trend with the increase in rolling deformation as shown in Table I. This conclusion is consistent with Fig. 4.

The metallographic structure of Zn–Cu–Ti alloy is mainly composed of black phase ($CuZn_5$) and white matrix (η phase) [see Fig. 4]. The value of Integral Optical Density (IOD) of ε phase ($CuZn_5$) was used to characterize the content of ε phase ($CuZn_5$). It is to make a quantitative analysis of deformation-induced precipitation of ε phase ($CuZn_5$) with the increase in rolling deformation.

https://doi.org/10.1557/jmr.2017.275 Published online by Cambridge University Press

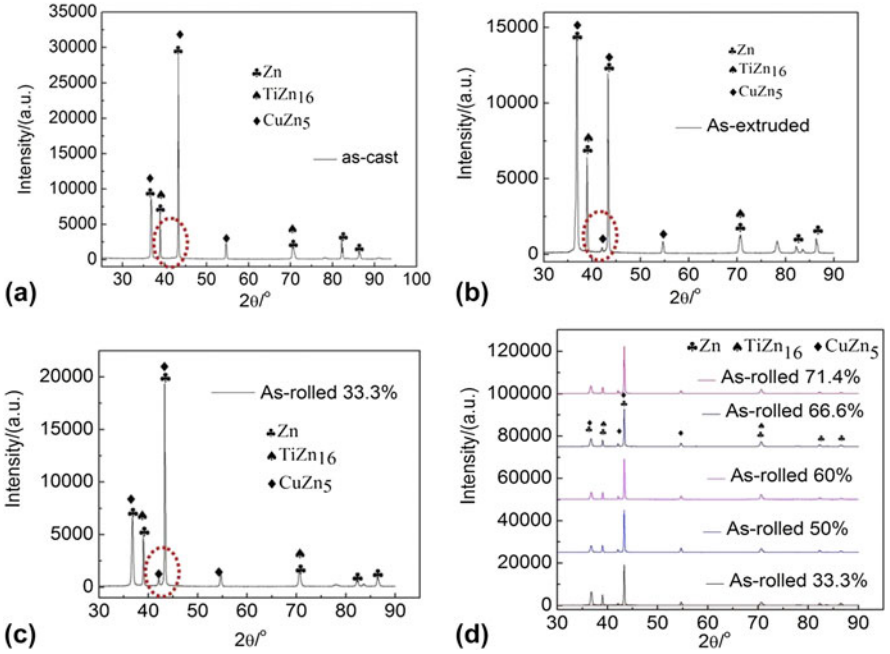


FIG. 5. (a) XRD pattern of as-cast Zn–Cu–Ti alloy, (b) XRD pattern of as-extruded Zn–Cu–Ti alloy, (c) XRD pattern of as-rolled Zn–Cu–Ti alloy, and (d) XRD pattern of as-rolled Zn–Cu–Ti alloy with different hot-rolling deformations.

TABLE I. Intensity of new diffraction peaks of ε phase of Zn–Cu–Ti alloy with different hot-rolling deformations.

Deformation (%)	33.3%	50%	60%	66.6%	71.4%
Intensity	658.51	1298.43	1537.77	1563.08	1594.35

TABLE II. The state parameter statistics of ε phase of Zn–Cu–Ti alloy at 300 °C.

Deformation (%)	Total area (μm^2)	Area percentage (%)	IOD
33.3	800.57	0.212	17,398.28
50	917.08	0.243	17,873.58
60	851.13	0.226	18,708.58
66.6	1032.85	0.274	19,932.34
71.4	1104.00	0.293	21,694.33

Table II shows a series of state parameters of ε phase ($CuZn_5$) of hot-rolled Zn–Cu–Ti alloy sheets at 300 °C. As shown in Table II, with the increase in hot-rolling deformation, amounts of deformation-induced precipitation of ε phase ($CuZn_5$) showed a rising trend.

According to the phase transition thermodynamics,[27] all systems have a tendency to change from high free energy to low free energy to achieve a stable state. The solid-state phase transition of metals is actually a spontaneous process of high free energy to low free energy. The driving force of the solid-state phase transition is the free energy difference between the new phase and the old phase. The activation energy of the solid-state phase transition needs to overcome the gravitation between atoms caused by lattice changes (Van der Waals force), the interfacial energy difference between the new phase and the old phase, elastic strain energy (caused by the volume difference of new phase and the matrix), and so on.

The more severe hot-rolling deformation, the more deformation-induced precipitation of ε phase ($CuZn_5$). This is because, on the one hand, the higher strain rate of the alloy during the process of plastic deformation, the greater deformation stored energy. It accelerates the nucleation of DRX. Meanwhile, the grain size in the matrix (η phase) is refined as well. The grain refinement expands the total grain boundary surface area of the matrix (η phase), which leads to the increase in the free energy of the matrix (η phase). When the increase in the free energy of the matrix (η phase) is greater than that in the free energy of ε phase ($CuZn_5$), it is beneficial to the deformation-induced precipitation of ε phase ($CuZn_5$). On the other hand, the variation of interatomic distance in the matrix, mismatch rise caused by lattice distortion, and transition from coherent interface to semicoherent interface (or incoherent interface) will lead to the increase in interfacial energy of the matrix (η phase). Free energy of the matrix (η phase) is released due to nucleation and precipitation of the local ε phase ($CuZn_5$). Furthermore, the increase in hot-rolling deformation leads to the increase in solute diffusion ability, which is also helpful to ε phase ($CuZn_5$) nucleation.

As shown in Fig. 6(a), deformation-induced precipitation of ε phase ($CuZn_5$) mainly existed in the grain boundaries of the matrix (η phase). It shows that deformation-induced precipitation of ε phase ($CuZn_5$)

https://doi.org/10.1557/jmr.2017.275 Published online by Cambridge University Press

was easier to nucleate in the grain boundaries.[28] This can be attributed to more dislocations, holes, and impurity atoms in the grain boundaries, which can lead to the increase of the supersaturation degree in the grain boundaries. In addition, the lattice distortion and the interface energy were increased by the disordered arrangement of atoms in the grain boundaries.

According to Cottrell's Air Mass Theory, solute atoms aggregate near the dislocation lines because of interactions between solute atoms and dislocations.[29,30] It is beneficial for ε phase ($CuZn_5$) to nucleate near the dislocation lines in the matrix (η phase). Meanwhile, the strain energy caused by dislocation movement decreases. It is due to nucleation of ε phase ($CuZn_5$) near the dislocation lines.[31] As shown in Figs. 6(a) and 6(b), it is also the reason that deformation-induced precipitation of ε phase ($CuZn_5$) still existed in the interior of grains in the matrix (η phase). By contrast of Figs. 6(a) and 6(b), with the increase in hot-rolling deformation, deformation-induced precipitation of ε phase ($CuZn_5$) in the interior of grains in the matrix (η phase) was increased. This is because the more severe the plastic deformation, the more the movement and proliferation of dislocations in the alloy, and the more the aggregated solute atoms caused by dislocations. It is more conducive to nucleation of ε phase ($CuZn_5$).

As shown in Figs. 6(c)–6(e), with medium and high deformation rates (60, 66.6, 71.4%), ε phase ($CuZn_5$) is nucleated and grows only in the grain boundaries. But it could not be visible within the grains. This is attributed to the rising ratio of DRX with increase in deformation. Dynamic recrystallization reduced the concentration of dislocations and vacancies in the grain interior. In addition, due to the reduction of interaction between solute atoms and dislocations in matrix (η phase), the probability of solute atoms segregation under edge dislocation was cut down. When the deformation reached 71.4%, deformation storage energy could be improved to a certain extent, and new nucleation and growth occurred in the interior of dynamic recrystallization grains again.[10] New undistorted equiaxed grains were generated. The probability of solute-atoms segregation

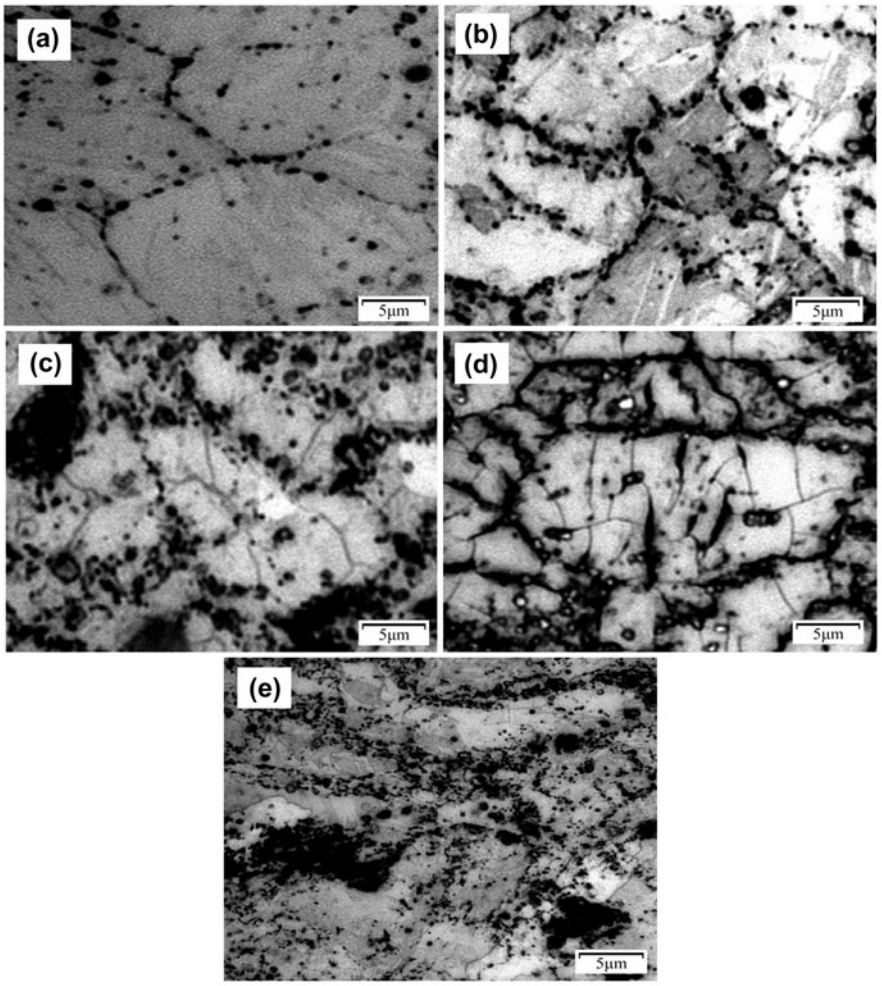


FIG. 6. OM micrographs of deformation-induced precipitation of ε phase with different rolling deformations: (a) 33.3%, (b) 50%, (c) 60%, (d) 66.6%, and (e) 71.4%.

https://doi.org/10.1557/jmr.2017.275 Published online by Cambridge University Press

under edge dislocation was further reduced, which decreased the possibility of ε phase ($CuZn_5$) nucleation in the interior of dynamic recrystallized grains.

D. Mechanical properties

Table III is the corresponding value of Fig. 7. It can be seen from Table III that the elongation rate of Zn–Cu–Ti alloys displays a wave shape: first rising, then falling, and later rising again with the increase in hot-rolling deformation. This is mainly because the ratio of DRX and deformation twins in the alloy correspondingly rises with the increase in the hot-rolling deformation. It makes the average grain size in the matrix (η phase) become smaller, which improves elongation rate of the alloy.

When the deformation reached 66.6%, ε phase ($CuZn_5$) is completely dispersed in the matrix, and its morphology became more tiny globe-like and granular. The continuous or discontinuous network of ε phase ($CuZn_5$) is distributed on the grain boundary of the matrix (η phase) [see Figs. 4(d) and 6(d)], which could lead to the decrease of the elongation rate of the alloy.

When the deformation reached 71.4%, the ratio of DRX and deformation twins was not only increased, but secondary DRX was induced. It also contributed to the further refinement of grains in Zn–Cu–Ti alloys. At the same time, the degree of dispersion of ε phase ($CuZn_5$) in the matrix (η phase) was further decreased. All of the factors led the maximum value of elongation rate of the alloy to reach 32.8% at the 71.4% of hot-rolling deformation.

TABLE III. Effects of different hot-rolling deformations on the tensile properties of Zn–Cu–Ti alloy at 300 °C.

Deformation (%)	33.3%	50%	60%	66.6%	71.4%
δ (%)	14.8	19.31	31.83	26.34	32.8
σ_b (MPa)	283.11	283.27	270.70	264.91	248.92

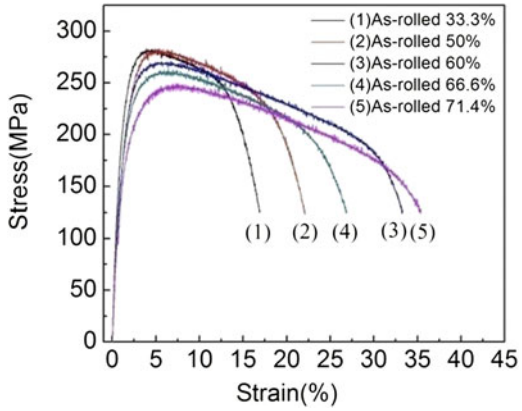


FIG. 7. Stress–strain curves during different hot-rolling deformations at 300 °C.

It can be seen from Table II that with the increase in hot-rolling deformation, the amount of deformation-induced precipitation of ε phase ($CuZn_5$) shows a rising trend. It lowers the solubility of copper in matrix (η phase) and weakens its solid-solution strengthening effect. It leads to the decrease in the tensile strength of Zn–Cu–Ti alloys with the increase in hot-rolling deformation [see Table III]. So, the solid-solution strengthening effect of copper plays an important role in the strengthening effect of Zn–Cu–Ti alloys. Furthermore, grain refinement caused by DRX and twins does not improve the tensile strength of Zn–Cu–Ti alloys. It is thus clear that the fine grain-strengthening effect plays a minor role in the intensity index of Zn–Cu–Ti alloys.

IV. CONCLUSIONS

(1) TEM analysis showed that twin deformation and (DRX) are two important deformation modes of Zn–Cu–Ti alloys during hot rolling at 300 °C. Twin deformation and DRX appear one after the other. They not only consume the deformation-stored energy but also inhibit the initiation and growth of cracks, which makes severe hot-rolling deformation possible.

(2) Under the condition of small deformations (33.3–60%), CDRX and DDRX are the main deformation mechanisms, complemented with twin deformation at the early stage of deformation. Under the condition of medium and high deformations (66.6–71.4%), twin deformation and TDRX are the main deformation mechanisms. The ratio of DRX and twins is increased with the increase in hot-rolling deformation. In addition, higher deformation stored energy is produced by the severe plastic deformation, which induces secondary DRX. It also contributes to the further refinement of grains in the matrix (η phase).

(3) The elongation rate of Zn–Cu–Ti alloys has a rising trend with the increase in hot-rolling deformation. It is mainly due to grain refinement caused by increasing the ratio of DRX and twins in the matrix (η phase). When the deformation reaches 66.6%, the continuous or discontinuous network of ε phase ($CuZn_5$) distributes in the grain boundaries of the matrix (η phase), which can lead to the decrease of the elongation rate of the alloy.

(4) The tensile strength of Zn–Cu–Ti alloys is found to decrease with the increase in hot-rolling deformation. This is because solid-solution strengthening effect of copper is weakened by more deformation-induced precipitation of ε phase ($CuZn_5$). The solid-solution strengthening effect of copper plays an important role in the strengthening effect of Zn–Cu–Ti alloys.

ACKNOWLEDGMENTS

This work was supported by the following projects: State Key Program of National Natural Science

https://doi.org/10.1557/jmr.2017.275 Published online by Cambridge University Press

Foundation of China (No. U1502274), Innovation Scientists and Technicians Troop Construction Projects of Henan Province (No. C20150014), Program for Innovation Research Team (in Science and Technology) in Universities of Henan Province (No. 14IRTSTHN007) and Key Scientific Program of Henan Province (No. 16A430004). We are indebted to the anonymous reviewers for their valuable comments and suggestions.

REFERENCES

1. A. Fata, G. Faraji, M.M. Mashhadi, and V. Tavakkoli: Hottensile deformation and fracture behavior of ultrafine-grained AZ31 magnesium alloy processed by severe plastic deformation. *Mater. Sci. Eng., A* **674**, 9 (2016).
2. F. Du, S. Yadav, C. Moreno, T.G. Murthy, and C. Saldana: Incipient straining in severe plastic deformation methods. *J. Mater. Res.* **29**(5), 718 (2014).
3. W.J. Huang, Z.Y. Liu, M. Lin, X.W. Zhou, L. Zhao, A.L. Ning, and S.M. Zeng: Reprecipitation behavior in Al–Cu binary alloy after severe plastic deformation-induced dissolution of θ′ particles. *Mater. Sci. Eng., A* **546**, 26 (2012).
4. T. Li, D. Kent, G. Sha, M.S. Dargusch, and J.M. Cairney: Precipitation of the α-phase in an ultrafine grained beta-titanium alloy processed by severe plastic deformation. *Mater. Sci. Eng., A* **605**, 144 (2014).
5. R. Kaibyshev, K. Shipilova, F. Musin, and Y. Motohashi: Continuous dynamic recrystallization in an Al–Li–Mg–Sc alloy during equal-channel angular extrusion. *Mater. Sci. Eng., A* **396**(1–2), 341 (2005).
6. L.M. Yan, J. Shen, J.P. Li, Z.B. Li, and Z.L. Tang: Dynamic recrystallization of 7055 aluminum alloy during hot deformation. *Mater. Sci. Forum* **650**, 295 (2010).
7. J. Liu, Z. Cui, and C. Li: Modelling of flow stress characterizing dynamic recrystallization for magnesium alloy AZ31B. *Comput. Mater. Sci.* **41**(3), 375 (2008).
8. S.V. Murty, S. Torizuka, K. Nagai, T. Kitai, and Y. Kogo: Dynamic recrystallization of ferrite during warm deformation of ultrafine grained ultra-low carbon steel. *Scr. Mater.* **53**(6), 763 (2005).
9. A. Gobrecht, R. Bendoula, J.M. Roger, and V. Bellon-Maurel: Combining linear polarization spectroscopy and the Representative Layer Theory to measure the Beer–Lambert law absorbance of highly scattering materials. *Anal. Chim. Acta* **853**(1), 486 (2015).
10. J.S. Pan: *Foundations of Materials Science* (Tsinghua University Press, Bejing, 1998).
11. Z.S. Hou and G.Z. Lu: *Principles of Metallography* (Shanghai Science and Technology Press, Shanghai, 1995).
12. S. Gourdet and F. Montheillet: A model of continuous dynamic recrystallization. *Acta Mater.* **51**(9), 2685 (2003).
13. Y.Q. Ning and Z.K. Yao: Recrystallization nucleation mechanism of FGH4096 powder metallugry superalloy. *Acta Metall. Sin.* **48**(8), 1005 (2012).
14. K. Jiang and S.J. Sun: Research of dynamic recrystallization critical criterion and mechanism. *Nonferrous Met. Process.* **38**(1), 25 (2010).
15. A. Serra and D.J. Bacon: Computer simulation of twinning dislocation in magnesium using a many-body potential. *Philos. Mag. A* **63**(5), 1001 (1991).
16. E.I. Galindo-Nava and P.E.J. Rivera-Díaz-Del-Castillo: Grain size evolution during discontinuous dynamic recrystallization. *Scr. Mater.* **72–73**(1), 1 (2014).
17. A. Momeni, G.R. Ebrahimi, M. Jahazi, and P. Bocher: Microstructure evolution at the onset of discontinuous dynamic recrystallization: A physics-based model of subgrain critical size. *Alloys Compd.* **587**(7), 199 (2014).
18. Z.X. Wu, Y.W. Zhang, and D.J. Srolovitz: Dislocation–twin interaction mechanisms for ultrahigh strength and ductility in nanotwinned metals. *Acta Mater.* **57**(15), 4508 (2009).
19. Y.T. Zhu, X.L. Wu, X.Z. Liao, J. Narayan, L.J. Kecskés, and S.N. Mathaudhu: Dislocation–twin interactions in nanocrystalline fcc metals. *Acta Mater.* **59**(2), 812 (2011).
20. J. Tu: *Deformation Twins and Twinning Mechanism of Hexagonal Close-Packed Met Under Dynamic Plastic Deformation* (Chongqing University, Chongqing, 2013).
21. A. Belyakov, H. Miura, and T. Sakai: Dynamic recrystallization under warm deformation of a 304 type austenitic stainless steel. *Mater. Sci. Eng., A* **255**(1–2), 139 (1998).
22. H. Miura, T. Sakai, H. Hamaji, and J.J. Jonas: Preferential nucleation of dynamic recrystallization at triple junctions. *Scr. Mater.* **50**(1), 65 (2004).
23. Y.N. Wang and J.C. Huang: Review: Texture analysis in hexagonal materials. *Mater. Chem. Phys.* **81**(1), 11 (2003).
24. I. Ulacia, N.V. Dudamell, F. Gálvez, S. Yi, M.T. Pérez-Prado, and I. Hurtado: Mechanical behavior and microstructural evolution of a Mg AZ31 sheet at dynamic strain rates. *Acta Mater.* **58**(8), 2988 (2010).
25. S.B. Yi, C.H.J. Davies, H.G. Brokmeier, R.E. Bolmaro, K.U. Kainer, and J. Homeyer: Deformation and texture evolution in AZ31 magnesium alloy during uniaxial loading. *Acta Mater.* **54**(2), 549 (2006).
26. J. Koike, T. Kobayashi, T. Mukai, H. Watanabe, M. Suzuki, K. Maruyama, and K. Higashi: The activity of non-basal slip systems and dynamic recovery at room temperature in fine-grained AZ31B magnesium alloys. *Acta Mater.* **51**(7), 2055 (2003).
27. J.R. Chen and C.J. Li: *Solid State Phase Transition in Metals and Alloys* (Metallurgical Industry Press, Bejing, 1997).
28. J. Li: *Study on the Microstructure Evolution and Precipitation Behaviors during Hot Charging Process for HSLA Steel* (Chongqing University, Chongqing, 2013).
29. D.K. Shi: *Foundations of Materials Science* (Machinery Industry Press, Bejing, 2003).
30. P. Liu: *Study of the Dislocation Dynamics in the Plastic Deformation* (Hefei University of Technology, Hefei, 2010).
31. H.J. Wang, B. Fu, L. Xiang, and S.T. Chou: Nucleation mechanism of precipitate of AlN in ferrite phase of Hi–B steel. *J. Iron Steel Res.* **27**(10), 40 (2015).

https://doi.org/10.1557/jmr.2017.275 Published online by Cambridge University Press